RESEARCH PAPER

Quality by Design-Based Optimization of Betamethasone Dipropionate-Loaded Nanostructured Lipid Carrier Nanogel for Topical Anti-Inflammatory Drug Delivery

Sonali Aher[1*], Dr. Nitin Jain[2], Dr. Usha Jain[3], Mr. Dadasaheb Kawade[4], Shraddha Kamankar[5]

[1,5]Department of Pharmaceutical Quality Assurance, Rashtrasant Janardhan Swami College of Pharmacy, Kokamthan, Tal- Kopargaon, Dist. Ahilyanagar, Maharashtra, 423601, India

[2,3,4]Department of Pharmaceutical Chemistry, Rashtrasant Janardhan Swami College of Pharmacy, Kokamthan, Tal- Kopargaon, Dist. Ahilyanagar, Maharashtra, 423601, India

Address for Correspondence:
Sonali Aher*
Address: Department of Pharmaceutical Quality Assurance, Rashtrasant Janardhan Swami College of Pharmacy, Kokamthan, Tal- Kopargaon, Dist. Ahilyanagar, Maharashtra, 423601, India
E-mail-Id: sonalia949@gmail.com

Received: 4th May, 2026; Revised: 18th May 2026; Accepted: 23th Jun, 2026; Available Online: 10th July, 2026

ABSTRACT:

Background: Conventional topical corticosteroid formulations, including creams and ointments, suffer from critical limitations such as poor skin penetration, inadequate drug localization in target tissue, and dose-dependent systemic side effects including hypothalamic-pituitary-adrenal (HPA) axis suppression and skin atrophy. Betamethasone dipropionate (BDP), a potent class III/IV corticosteroid, is widely employed in the management of inflammatory dermatoses; however, existing marketed formulations fail to achieve optimal therapeutic outcomes due to these physicochemical and pharmacokinetic constraints.

Objective: This study aimed to develop and systematically optimize BDP-loaded nanostructured lipid carrier (NLC)based nanogel using a Quality by Design (QbD) approach to maximize topical bioavailability, enhance skin permeation, and sustain drug release while minimizing systemic absorption.

Methods: A comprehensive QbD framework encompassing Target Product Profile (QTPP), Critical Quality Attributes (CQAs), and risk assessment via Ishikawa fishbone analysis was established. A three-factor, three-level Box-Behnken Design (BBD) was employed to optimize critical material attributes: solid lipid concentration (X1), liquid lipid concentration (X2), and surfactant concentration (X3). NLCs were prepared by hot melt emulsification-ultrasonication and incorporated into Carbopol 934P nanogel. Formulations were characterized for particle size, polydispersity index (PDI), zeta potential, entrapment efficiency (EE%), drug release, viscosity, spreadability, ex vivo skin permeation, in vivo anti-inflammatory activity (carrageenan paw edema model), and stability.

Results: The optimized BDP-NLC exhibited particle size of 168.4 ± 3.2 nm, PDI of 0.19 ± 0.02, zeta potential of −31.2 ± 1.4 mV, and EE% of 87.3 ± 1.8%. The nanogel demonstrated pseudoplastic flow, viscosity of 9,840 ± 420 cPs, and spreadability of 15.2 ± 0.8 g·cm/s. Ex vivo permeation studies revealed a 3.2-fold enhancement in flux compared to marketed Diprolene® cream. In vivo studies demonstrated 71.4 ± 3.1% edema inhibition at 4 hours. Stability studies confirmed ICH Q1A(R2) compliance over 6 months under accelerated conditions.

Conclusion: The QbD-optimized BDP-NLC nanogel constitutes a superior topical drug delivery platform offering enhanced permeation, sustained release, and improved anti-inflammatory efficacy relative to conventional marketed formulations, with potential to reduce systemic corticosteroid side effects.

KEYWORDS: Betamethasone Dipropionate, Nanostructured Lipid Carriers (NLCs), Quality by Design (QbD), Topical Drug Delivery

How to cite this article: Aher S, Jain N, Jain U, Kawade D, Kamankar S. Quality by Design-Based Optimization of Betamethasone Dipropionate-Loaded Nanostructured Lipid Carrier Nanogel for Topical Anti-Inflammatory Drug Delivery. Int J Drug Deliv Technol. 2026;16(66s):1454-1470. DOI: 10.25258/ijddt.16.66s.156

INTRODUCTION:

Skin as a Drug Delivery Barrier

The skin is the largest organ of the human body, covering approximately 1.8 m² in the average adult, and functions as a sophisticated multilayered barrier against chemical, physical, and biological insults. For topical drug delivery, the skin simultaneously serves as the target tissue and the primary obstacle to therapeutic intervention. A thorough understanding of its architecture is fundamental to rational formulation design.

The skin is organized into three principal layers: the epidermis, dermis, and hypodermis. The outermost layer of the epidermis, the stratum corneum (SC), comprises 15–20 layers of flattened, anucleated corneocytes embedded in a continuous lipid matrix of ceramides, cholesterol, and free fatty acids often described using the 'brick and mortar' model. This organized lipid bilayer architecture confers the SC's exceptional impermeability, rendering it the ratelimiting barrier for most topically applied drugs. The SC's thickness ranges from 10 to 15 μm on most body sites but can reach up to 400–600 μm on the palms and soles.

Drug molecules may traverse the SC via three principal pathways: (i) the transcellular (intracellular) route, passing directly through corneocytes and intercellular lipids; (ii) the intercellular (extracellular) route, diffusing through the tortuous lipid domains between corneocytes the predominant pathway for most drugs; and (iii) the transappendageal route, bypassing the SC via hair follicles and eccrine sweat ducts. Although appendages occupy only 0.1% of the total skin surface, follicular penetration is particularly relevant for nanoparticulate systems, which can accumulate preferentially in follicular orifices.

The viable epidermis beneath the SC contains keratinocytes, Langerhans cells, and melanocytes, and provides additional resistance due to its aqueous character. The dermis, a richly vascularized connective tissue layer, contains fibroblasts, mast cells, and the microcirculatory network responsible for systemic drug absorption an undesirable outcome in topical anti-inflammatory therapy. NLC-based nanogels are specifically engineered to enhance drug deposition in the epidermal and upper dermal compartments while limiting dermal vascular absorption.

Betamethasone Dipropionate Drug Profile

Betamethasone dipropionate (BDP; INN: betamethasone 17,21-dipropionate) is a synthetic fluorinated glucocorticoid ester classified as a potent (class III) to very potent (class IV) topical corticosteroid according to the WHO/ECSS classification system. It is the dipropionic acid diester of betamethasone, a 9α-fluoro, 16β-methyl prednisolone derivative that exhibits markedly enhanced receptor affinity and lipophilicity relative to hydrocortisone.

Mechanistically, BDP exerts its anti-inflammatory effects primarily through binding to cytosolic glucocorticoid receptors (GRs), which translocate to the nucleus upon ligand binding and modulate gene transcription. Key anti-inflammatory mechanisms include: (i) inhibition of phospholipase A2 (PLA2) via induction of lipocortin/annexin I, thereby suppressing arachidonic acid liberation and downstream prostaglandin/leukotriene synthesis; (ii) downregulation of pro-inflammatory cytokines including IL-1β, IL-6, TNF-α, and IFN-γ through transrepression of NF-κB and AP-1 transcription factors; and (iii) reduction of vascular permeability, vasoconstriction, and inhibition of leucocyte migration.

Therapeutically, BDP is indicated for a broad spectrum of inflammatory dermatoses including psoriasis vulgaris, atopic dermatitis, contact dermatitis, nummular eczema, lichen planus, and seborrheic dermatitis. Its physicochemical properties include a molecular weight of 504.6 g/mol, a log P value of approximately 3.5 indicating significant lipophilicity, a melting point of 178–181°C, and practically negligible aqueous solubility (<0.05 mg/mL at 25°C). While lipophilicity favors partitioning into the SC lipid matrix, the high molecular weight and poor aqueous solubility limit its flux through the viable epidermis.

Marketed formulations of BDP include Diprolene® (0.05% augmented betamethasone dipropionate) and Diprosalic® (0.05% BDP + 3% salicylic acid). These conventional preparations are associated with significant local and systemic adverse effects with prolonged use, including: cutaneous atrophy, striae distensae, telangiectasia, tachyphylaxis, acneiform eruptions, and HPA axis suppression manifesting as Cushing's syndrome in severe cases. These limitations underscore the urgent need for innovative delivery systems capable of enhancing localized drug action while curtailing systemic bioavailability.

Nanostructured Lipid Carriers Rationale and Advantages

The evolution of lipid-based nanocarriers for topical drug delivery reflects a progressive refinement of formulation science: from simple oil-in-water emulsions through solid lipid nanoparticles (SLNs) to the current generation of nanostructured lipid carriers (NLCs). SLNs, developed in the early 1990s, comprise a solid lipid matrix at physiological temperature, offering controlled release and improved stability over emulsions. However, the highly ordered crystalline

structure of solid lipids limits drug loading capacity and leads to drug expulsion upon lipid polymorphic transitions during storage.

NLCs overcome these inherent limitations through the deliberate incorporation of a liquid lipid (oil) component into the solid lipid matrix. The spatial incompatibility between solid and liquid lipid molecules disrupts the crystal lattice, creating an amorphous or imperfect crystalline structure with numerous structural defects that accommodate higher drug loading and prevent drug expulsion during storage. Three distinct NLC structural subtypes are recognized: Type I (imperfect type) in which the liquid lipid is molecularly dispersed within the solid lipid lattice, generating crystalline imperfections; Type II (amorphous type) in which the lipid mixture does not crystallize upon solidification, forming an amorphous matrix; and Type III (multiple type) in which the liquid lipid forms discrete oil nanodomains within the solid lipid matrix. This study employs a Type I imperfect NLC architecture, as it maximizes drug solubilization while maintaining adequate solid-state integrity. The skin penetration enhancement mechanisms operative in NLC-mediated topical delivery are multifactorial. First, the small particle size (<200 nm) of NLCs enables follicular penetration and accumulation in perifollicular regions, providing a depot for sustained drug release. Second, the occlusive effect of the solid lipid film deposited on the SC surface increases hydration of the cornified layers, disrupting corneocyte packing and enhancing drug diffusion. Third, the lipid components of NLCs, particularly oleic acid, interact with SC lipid bilayers to increase membrane fluidity and reduce the diffusional resistance of the intercellular lipid domains. Collectively, these mechanisms confer significant permeation enhancement without the chemical irritation associated with conventional penetration enhancers.

NLC Nanogel Concept and Rationale

While NLC dispersions exhibit superior drug delivery characteristics, their liquid colloidal nature limits practical topical application due to poor cosmetic acceptability, inadequate residence time on the application site, and the risk of dripping or migration to unintended areas. Conversion of the NLC dispersion into a semi-solid gel matrix addresses these limitations by providing appropriate consistency, prolonged contact time, and patient acceptability. The choice of gelling agent significantly influences the physicochemical and performance characteristics of the resulting nanogel. Carbopol 934P (crosslinked polyacrylic acid polymer) was selected as the gelling agent in this study based on its well-established safety profile, ability to form transparent gels at low concentrations (0.5–2.0% w/w), pH-dependent viscosity (requiring neutralization to pH 6.5–7.0 with triethanolamine), bioadhesive properties that enhance epidermal contact time, and compatibility with NLC components. Alternative gelling agents considered included hydroxypropyl methylcellulose (HPMC) and Poloxamer 407; however, Carbopol 934P was preferred for its superior pseudoplastic rheological behavior and established regulatory acceptance.

Quality by Design in Pharmaceutical Development

Quality by Design (QbD), as defined by the ICH Q8(R2) guideline, is 'a systematic approach to development that begins with predefined objectives and emphasizes product and process understanding and process control, based on sound science and quality risk management.' The QbD paradigm represents a fundamental departure from the traditional empirical 'quality by testing' approach, offering instead a knowledge-driven framework that identifies the design space within which product quality is assured.

The QbD workflow is structured as a sequential, iterative process: definition of the Quality Target Product Profile (QTPP) establishing the desired performance attributes of the final product; identification of Critical Quality Attributes (CQAs) that must be within specified limits to ensure product quality; risk assessment (using tools such as Ishikawa cause-and-effect diagrams and risk priority number matrices) to identify Critical Process Parameters (CPPs) and Critical Material Attributes (CMAs) that most significantly impact CQAs; Design of Experiments (DoE) to systematically explore the multivariate design space; derivation of a Design Space defining the multidimensional combination of input variables that assures quality; and establishment of a Control Strategy to maintain the process within the design space. This structured approach, endorsed by ICH Q8/Q9/Q10 guidelines and FDA guidance on pharmaceutical development, facilitates regulatory acceptance and process robustness. Design of Experiments, specifically the Box-Behnken Design (BBD), is employed in this study to efficiently explore the response surface and identify optimal formulation conditions. BBD is a three-level incomplete factorial design that evaluates all factors at intermediate levels simultaneously, eliminating extreme corner points that may be physically impractical or undesirable. The BBD allows fitting of a second-order (quadratic) polynomial response surface model, enabling prediction of response values across the entire design space with a minimum number of experimental runs.

MATERIALS AND METHODS:

Materials

Betamethasone dipropionate (BDP, purity >99.5%) was obtained as a gift sample from Glenmark Pharmaceuticals Ltd., Compritol 888 ATO (glyceryl dibehenate, solid lipid) was procured from Gattefossé SAS. Oleic acid (liquid lipid, pharmaceutical grade) was purchased from Sigma-Aldrich. Polysorbate 80 (Tween 80, HLB 15.0) and Sorbitan monooleate (Span 80, HLB 4.3) were obtained from HiMedia

Laboratories Pvt. Ltd., Poloxamer 188 was supplied by BASF SE, Ludwigshafen. Carbopol 934P (crosslinked carbomer homopolymer, viscosity grade) was gifted by Lubrizol Advanced Materials India Pvt. Ltd. Triethanolamine (TEA, analytical grade) and polyethylene glycol 400 (PEG 400) were purchased from Merck KGaA. Phosphate-buffered saline (PBS) components (monobasic and dibasic sodium phosphate, sodium chloride) of analytical reagent grade were procured from Qualigens Fine Chemicals. Diprolene® cream 0.05% (augmented betamethasone dipropionate) was obtained commercially. All other chemicals and solvents were of analytical or HPLC grade. Double-distilled water (specific resistance > 18 MΩ·cm) was used throughout all experiments. Betamethasone dipropionate (BDP, purity >99.5%) was obtained as a gift sample from Glenmark Pharmaceuticals Ltd., Mumbai, Maharashtra, India. Compritol 888 ATO (glyceryl dibehenate, solid lipid) was procured from Gattefossé SAS, Saint-Priest, France. Oleic acid (liquid lipid, pharmaceutical grade) was purchased from Sigma-Aldrich, St. Louis, MO, USA. Polysorbate 80 (Tween 80, HLB 15.0) and Sorbitan monooleate (Span 80, HLB 4.3) were obtained from HiMedia Laboratories Pvt. Ltd., Mumbai, Maharashtra, India. Poloxamer 188 was supplied by BASF SE, Ludwigshafen, Germany. Carbopol 934P (crosslinked carbomer homopolymer, viscosity grade) was gifted by Lubrizol Advanced Materials India Pvt. Ltd., Mumbai, Maharashtra, India. Triethanolamine (TEA, analytical grade) and polyethylene glycol 400 (PEG 400) were purchased from Merck KGaA, Darmstadt, Germany. Phosphatebuffered saline (PBS) components (monobasic and dibasic sodium phosphate, sodium chloride) of analytical reagent grade were procured from Qualigens Fine Chemicals, Mumbai, Maharashtra, India. Diprolene® cream 0.05% (augmented betamethasone dipropionate) was obtained commercially as a reference standard. All other chemicals and solvents used were of analytical or HPLC grade. Double-distilled water with a specific resistance greater than 18 MΩ·cm was used throughout all experiments.

QbD Framework

Quality Target Product Profile (QTPP)

The QTPP for the BDP-NLC nanogel was defined as a semi-solid, opaque-to-translucent nanogel formulation intended for topical application to skin affected by inflammatory dermatoses (atopic dermatitis, psoriasis, eczema). The target drug concentration was 0.05% w/w BDP, consistent with marketed reference products. The intended release pattern was biphasic (initial rapid release for acute symptom relief followed by sustained release for prolonged therapeutic effect over 8 hours). The formulation was required to be physically and chemically stable under ICH Q1A(R2) conditions for a minimum of 24 months, with a pH in the range of 6.0–7.0 compatible with skin physiology.

Critical Quality Attributes (CQAs)

Based on the QTPP and risk assessment, the following CQAs were identified: particle size (PS, target <200 nm) influencing skin penetration depth and permeation rate; polydispersity index (PDI, target <0.25) reflecting colloidal homogeneity; zeta potential (ZP, target < −25 mV) indicating electrostatic colloidal stability; entrapment efficiency (EE%, target >85%) determining available drug payload; in vitro drug release at 8 hours (Q8h, target 70–80%); viscosity (target 8,000–12,000 cPs) governing spreadability; spreadability (target 12–20 g·cm/s); and ex vivo permeation flux (Jss) as a surrogate for in vivo performance.

Risk Assessment

A comprehensive risk assessment was conducted using an Ishikawa cause-and-effect (fishbone) diagram incorporating six M's (Materials, Methods, Machine, Man, Measurement, Mother Nature) to identify all potential sources of variability in CQAs. High-risk CMAs identified included: lipid composition (solid:liquid lipid ratio), surfactant type and concentration, drug concentration, and homogenization parameters. A risk priority number (RPN) matrix was constructed by scoring each variable for severity (1–10), occurrence (1–10), and detectability (1–10). Variables with RPN >100 were selected for inclusion in the DoE. Three independent variables emerged from risk assessment: solid lipid concentration (X1: Compritol 888 ATO, % w/w), liquid lipid concentration (X2: oleic acid, % w/w), and surfactant concentration (X3: Tween 80, % w/w).

Experimental Design Box-Behnken Design

A three-factor, three-level Box-Behnken Design (BBD) was implemented using Design-Expert® software version 13.0 (Stat-Ease Inc., Minneapolis, USA) to optimize the BDP-NLC formulation. The selected independent variables and their coded and actual levels are presented in Table 1. The design

generated 15 experimental runs, including 3 centerpoint replicates for pure error estimation. The dependent variables (responses) studied were Y1 (particle size, nm), Y2 (entrapment efficiency, %), and Y3 (drug release at 8 hours, %). A quadratic polynomial response surface model was fitted to each response:

$Y = \beta0 + \beta1X1 + \beta2X2 + \beta3X3 + \beta12X1X2 + \beta13X1X3 + \beta23X2X3 + \beta11X1^2 + \beta22X2^2 + \beta33X3^2$

where β0 is the intercept, β1–β3 are main effect coefficients, β12, β13, β23 are interaction coefficients, and β11, β22, β33 are quadratic coefficients. Model adequacy was evaluated by ANOVA, lack-of-fit test, coefficient of determination (R^2), adjusted R^2, predicted R^2, and adequate precision.

Table 1. Box-Behnken Design: Independent Variables and Their Levels

Variable	Low Level (−1)	Center Point (0)	High Level (+1)
X1: Compritol 888 ATO (% w/w)	2.0	3.5	5.0
X2: Oleic acid (% w/w)	0.5	1.25	2.0
X3: Tween 80 (% w/w)	0.5	1.25	2.0

Preparation of BDP-NLC

BDP-NLCs were prepared by hot melt emulsification followed by probe ultrasonication. The lipid phase was prepared by melting Compritol 888 ATO and oleic acid together in a glass beaker at 75 ± 2°C in a temperature-controlled water bath. BDP (0.05% w/w of total formulation weight) was dissolved in the molten lipid phase under continuous stirring (500 rpm) until a clear, homogeneous solution was obtained. The aqueous phase was prepared separately by dissolving Tween 80 (with or without Span 80 as co-surfactant, depending on the run) in double-distilled water preheated to 75 ± 2°C. The lipid phase was then added dropwise to the aqueous phase under high-speed homogenization at 10,000 rpm for 10 minutes using an Ultra-Turrax T25 homogenizer (IKA-Werke, Staufen, Germany) to form a coarse emulsion. The resulting hot emulsion was immediately subjected to probe ultrasonication (Vibra-Cell VCX 500, Sonics & Materials Inc., Newtown, USA) at 40% amplitude for 5 minutes in pulse mode (5 s on, 2 s off) while maintaining the temperature above the melting point of the lipid mixture (≥75°C). The hot nanoemulsion was subsequently cooled to room temperature (25°C) under gentle magnetic stirring (200 rpm) over 30 minutes to allow nanoparticle solidification. The resulting NLC dispersion was stored at 4°C until further use.

Preparation of NLC Nanogel

Carbopol 934P nanogels were prepared by dispersing the polymer (at concentrations of 0.5, 1.0, and 1.5% w/w) in double-distilled water with continuous stirring at 500 rpm for 12 hours at room temperature to ensure complete hydration and avoid polymer lump formation. The dispersion was then neutralized to pH 6.5–7.0 by dropwise addition of triethanolamine (10% v/v aqueous solution) under continuous stirring, which triggered gelation through ionization of carboxylic acid groups. The optimized BDP-NLC dispersion (containing 0.05% BDP) was then incorporated into the pre-formed Carbopol gel base at a 1:1 v/v ratio under gentle stirring at 200 rpm for 30 minutes to produce the NLC nanogel. The mixture was homogenized using a low-shear laboratory homogenizer at 500 rpm for 5 minutes. The final pH was verified and adjusted if necessary. Three gel concentrations (0.5, 1.0, and 1.5% Carbopol 934P w/w) were evaluated for rheological properties, and the optimal concentration was selected based on combined viscosity and spreadability criteria.

Characterization of BDP-NLC

Particle Size, PDI, and Zeta Potential

Particle size (mean hydrodynamic diameter), PDI, and zeta potential of BDP-NLC dispersions were determined by dynamic light scattering (DLS) using a Malvern Zetasizer Nano ZS instrument (Malvern Panalytical, Worcestershire, UK) equipped with a 4 mW He-Ne laser (λ = 633 nm) at a fixed scattering angle of 173° (non-invasive backscatter, NIBS technology). Samples were diluted 1:100 with filtered (0.22 μm) distilled water immediately before measurement to avoid multiple scattering. Zeta potential measurements were performed in disposable folded capillary zeta cells using electrophoretic light scattering (ELS). All measurements were performed at 25 ± 0.1°C in triplicate (n = 3) and results reported as mean ± standard deviation.

Entrapment Efficiency

EE% was determined by ultracentrifugation method. NLC dispersion (1 mL) was ultracentrifuged at 20,000 rpm for 30 minutes at 4°C using an Optima L-90K ultracentrifuge (Beckman Coulter, Brea, USA). The supernatant was carefully removed and the pellet was dissolved in methanol:acetonitrile (60:40 v/v). Total drug content was determined by dissolving an equivalent volume of NLC dispersion in methanol :acetonitrile. BDP concentration was measured by UV-Vis spectrophotometry at 239 nm (Shimadzu UV-1800,

Kyoto, Japan) against a calibrated standard curve (linearity: 1–50 µg/mL, R^2 = 0.9997). EE% was calculated as: EE% = [(Total drug − Free drug)/Total drug] × 100.

Transmission Electron Microscopy

The morphological characteristics of the optimized BDP-NLC were examined by transmission electron microscopy (TEM) using a JEOL JEM-2100F instrument (JEOL Ltd., Tokyo, Japan) operated at 200 kV accelerating voltage. For sample preparation, a drop of diluted NLC dispersion was placed on a carbon-coated copper grid (300 mesh) and allowed to adsorb for 2 minutes. Excess liquid was blotted with filter paper, and the grid was negatively stained with 2% phosphotungstic acid (PTA) solution for 30 seconds, dried at room temperature, and examined under the electron beam.

Thermal Analysis (DSC)

Differential scanning calorimetry (DSC) was performed using a DSC-60 Plus instrument (Shimadzu, Kyoto, Japan) calibrated with indium standard (melting onset 156.6°C, ΔH = 28.45 J/g). Samples of approximately 5–8 mg (pure BDP, Compritol 888 ATO, oleic acid, Tween 80, physical mixture, and freeze-dried BDP-NLC) were hermetically sealed in aluminum pans and scanned under nitrogen purge at a flow rate of 50 mL/min. The temperature program was: isothermal hold at 25°C for 2 minutes, ramp at 10°C/min from 25°C to 300°C. The crystallinity index (CI) of lipids in NLCs relative to bulk lipid was calculated as: CI (%) = [ΔH_NLC / ΔH_bulk lipid] × 100.

X-ray Powder Diffractometry (PXRD)

PXRD analysis was performed using a Bruker D8 Advance diffractometer (Bruker AXS GmbH, Karlsruhe, Germany) with CuKα radiation (λ = 1.5406 Å) generated at 40 kV and 40 mA. Samples were spread as thin films on a zero-background silicon sample holder and scanned over a 2θ range of 5°–50° at a step size of 0.02° and scan rate of 0.5°/min. Diffractograms of pure BDP, bulk lipids, physical mixture, and freeze-dried BDP-NLC were compared.

Fourier-Transform Infrared Spectroscopy (FTIR)

FTIR spectra were recorded using a Perkin-Elmer Frontier FTIR spectrometer (Perkin-Elmer Inc., Waltham, USA) in attenuated total reflectance (ATR) mode. Each spectrum was collected over the wavenumber range 4000–400 cm^{-1} as an average of 32 scans at 4 cm^{-1} resolution. Samples (pure BDP, lipid excipients, physical mixture, and freeze-dried BDPNLC) were analyzed without further preparation in ATR mode.

In Vitro Drug Release

In vitro drug release from BDP-NLC was studied using a two-chamber Franz diffusion cell system (PermeGear Inc., Hellertown, USA) with an effective diffusion area of 1.76 cm^2 and receptor volume of 12 mL. A pre-treated regenerated cellulose dialysis membrane (MWCO 12,000 Da, Sigma-Aldrich) was mounted between the donor and receptor chambers. The receptor compartment was filled with PBS pH 5.5 (simulating skin surface pH) containing 0.5% Tween 80 (to maintain sink conditions verified by solubility studies) maintained at 32 ± 0.5°C (skin surface temperature) under magnetic stirring at 600 rpm. BDP-NLC dispersion equivalent to 1 mg BDP was placed in the donor compartment. Aliquots of 1 mL were withdrawn at 0.5, 1, 2, 3, 4, 5, 6, 7, and 8 hours and replaced with equal volumes of fresh receptor medium. BDP concentration in withdrawn samples was quantified by HPLC. Cumulative percentage drug release was calculated and data were subjected to kinetic modeling (zero-order, first-order, Higuchi, and Korsmeyer-Peppas models).

Characterization of NLC Nanogel

The nanogel was evaluated for visual appearance, clarity, and homogeneity by visual inspection and optical microscopy. pH was measured using a calibrated digital pH meter (Mettler-Toledo FiveEasy Plus, Ohio, USA) with a flat-surface electrode directly inserted into the nanogel. Viscosity was measured at 25 ± 0.5°C using a Brookfield RV-DV-II+ Pro viscometer (Brookfield Engineering Laboratories, Stoughton, USA) equipped with spindle RV3 at 20 rpm after 60-second equilibration. Rheological behavior was characterized by measuring viscosity at shear rates from 1 to 100 rpm using the same instrument; flow curves were fitted to the HerschelBulkley model. Spreadability was measured by the glass slide method: 1 g of nanogel was sandwiched between two glass slides (10 × 10 cm) and a standard weight of 20 g was placed on the upper slide for 1 minute. The area of spread was measured and spreadability calculated as g·cm/s. Drug content uniformity was determined by extracting drug from 1 g of nanogel with methanol:acetonitrile (60:40 v/v), sonicating for 30 minutes, centrifuging, and analyzing the supernatant by HPLC.

HPLC Method Validation

A reverse-phase HPLC method was developed and validated for quantification of BDP in all samples. Chromatographic separation was achieved on a Phenomenex Luna C18 column (250 × 4.6 mm, 5 µm particle size, 100 Å pore size) at 30°C column temperature. The mobile phase consisted of acetonitrile:water (70:30 v/v) delivered isocratically at

a flow rate of 1.0 mL/min. Detection was performed at 239 nm using a UV-Vis detector (Shimadzu SPD20A). Injection volume was 20 µL. The method was validated per ICH Q2(R1) guidelines for specificity, linearity (2–100 µg/mL, R^2 = 0.9998), precision (intraday RSD <1.2%, inter-day RSD <2.1%), accuracy (98.8–101.5% recovery), LOD (0.48 µg/mL), and LOQ (1.46 µg/mL).

Ex Vivo Skin Permeation Study

Ex vivo skin permeation studies were conducted using rat abdominal skin obtained from male Wistar rats (200–250 g) after prior approval by the Institutional Animal Ethics Committee (IAEC) under Protocol No. IAEC/2024/Ph/012. Rats were sacrificed by cervical dislocation following anesthesia with ketamine/xylazine (90/10 mg/kg, i.p.), and abdominal skin was excised, shaved, and dermatomed to a uniform thickness of 400 ± 50 µm using a Dermatome (Zimmer, Warsaw, USA). Subcutaneous fat was carefully removed with a scalpel. Skin integrity was verified by transepidermal water loss (TEWL) measurement (Tewameter TM 300, Courage+Khazaka, Cologne, Germany); only specimens with TEWL <10 g/m²/h were used.

The excised skin was mounted on Franz diffusion cells (effective diffusion area: 1.76 cm²) with the SC surface facing the donor compartment. The receptor compartment contained PBS pH 7.4 supplemented with 20% v/v ethanol (to maintain sink conditions) at 32 ± 0.5°C with stirring at 600 rpm. After 30-minute equilibration, formulations containing equivalent drug doses (1 mg BDP) were applied to the SC surface. Comparative formulations included: BDP-NLC nanogel (optimized), plain drug gel (BDP in Carbopol 934P 1% nanogel without NLC), and marketed Diprolene® cream 0.05%. Samples (1 mL) were withdrawn at predetermined time points (1, 2, 3, 4, 5, 6, 7, 8 hours) and replaced with fresh receptor medium. BDP concentrations were determined by validated HPLC. Permeation parameters calculated included steady-state flux (Jss, µg/cm²/h, from slope of linear portion of cumulative permeation vs. time curve), lag time (Tlag, h, from x-intercept), permeability coefficient (Kp = Jss/C0), and enhancement ratio (ER = Jss of NLC nanogel/Jss of marketed cream).

Drug retention in skin layers was assessed by tapestripping at the end of the 8-hour permeation experiment. Sequential adhesive tape strips (Scotch® Crystal Clear, 3M, MN, USA) were applied to the SC surface and immediately removed. The first 5 strips were discarded (representing the outermost SC layers contaminated by residual formulation), and the subsequent 10 strips were collected. Drug was extracted from tape strips with methanol:acetonitrile and analyzed by HPLC. The remaining skin (viable epidermis + dermis) was minced, extracted in the same solvent system, sonicated for 30 minutes, centrifuged, and analyzed.

In Vivo Anti-Inflammatory Activity

The carrageenan-induced paw edema model in Wistar rats was employed to evaluate in vivo antiinflammatory efficacy, following approval by CPCSEA under Protocol No. CPCSEA/2024/102. Thirty male Wistar rats (150–200 g) were randomly allocated to five groups (n = 6 per group): Group I (Vehicle control, untreated), Group II (Carrageenan control, carrageenan + vehicle gel), Group III (Plain drug gel, carrageenan + BDP plain gel 0.05%), Group IV (Marketed cream, carrageenan + Diprolene® 0.05%), and Group V (BDP-NLC nanogel, carrageenan + optimized formulation 0.05%). Formulations (200 mg) were applied topically to the right hind paw (shaved 24 hours prior) 1 hour before subplantar injection of 0.1 mL of 1% w/v carrageenan (Type IV lambda; Sigma-Aldrich) in normal saline using a 26-gauge hypodermic needle. An additional application was made immediately after carrageenan injection. Paw volume was measured using a digital plethysmometer (Ugo Basile, Gemonio, Italy) at 0, 1, 2, 3, 4, 5, and 6 hours post-carrageenan injection. Percentage edema inhibition was calculated as: % Inhibition = [(Vt_control − Vt_treated)/Vt_control] × 100, where Vt is the increase in paw volume at time t. Statistical significance was evaluated by one-way ANOVA with Tukey's post-hoc test (GraphPad Prism 9.0). At the conclusion of the study (6 h), animals were sacrificed and paw tissues were harvested, fixed in 10% neutral buffered formalin, processed for histopathology using standard hematoxylin and eosin (H&E) staining, and examined under light microscopy.

Stability Studies

Stability of the optimized BDP-NLC nanogel was evaluated according to ICH Q1A(R2) guidelines under two conditions: accelerated stability (40°C ± 2°C / 75% RH ± 5% RH) and long-term stability (25°C ± 2°C / 60% RH ± 5% RH) for 6 months. Samples were stored in sealed amber glass vials in humidity chambers (Thermolab Scientific Equipments, Mumbai, India). At predetermined intervals (0, 1, 3, and 6 months), samples were withdrawn and analyzed for particle size, PDI, zeta potential, EE%, pH, viscosity, and drug content. Statistical significance of changes from baseline (T=0) was evaluated by paired t-test ($p < 0.05$).

RESULTS AND DISCUSSION:

Risk Assessment and QbD ramework

The QTPP established the BDPNLC nanogel as a 0.05% BDP semi-solid topical formulation with

targeted biphasic drug release, compatibility with skin pH (6.0–7.0), and 24-month shelf life. Seven CQAs were identified through QTPP analysis and expert knowledge: PS, PDI, ZP, EE%, Q8h drug release, viscosity, and spreadability. Risk assessment via Ishikawa fishbone analysis identified 18 potential CMAs and CPPs across the six categories. Among these, solid lipid concentration (X1), liquid lipid concentration (X2), and surfactant concentration (X3) received the highest RPN scores (RPN: 216, 192, and 168 respectively, threshold = 100) and were selected as independent variables for the DoE. Figure 1 depicts the risk ranking matrix with RPN distribution.

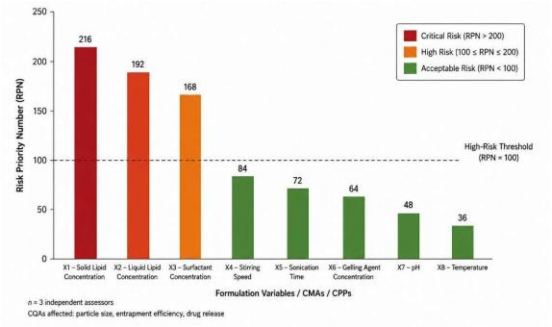

Figure 1: Risk Priority Number (RPN) matrix derived from Ishikawa fishbone analysis of BDPNLC nanogel formulation variables.

Box-Behnken Design: Experimental Results

The complete BBD experimental run matrix with measured responses (Y1: PS, Y2: EE%, Y3: Q8h drug release) is presented in Table 2. Particle size ranged from 136.2 nm (Run 7) to 284.6 nm (Run 12) across the 15 experimental runs. EE% ranged from 76.4% to 91.8%, and Q8h drug release from 62.3% to 85.7%.

Table 2. Box-Behnken Design Run Matrix with Experimental Responses for BDP-NLC Formulations

Run	X1 (% w/w)	X2 (% w/w)	X3 (% w/w)	Y1: PS (nm)	Y2: EE (%)	Y3: Q8h (%)
1	2.0	0.5	1.25	248.3± 4.2	78.6± 1.4	68.4± 1.8
2	5.0	0.5	1.25	271.5± 5.6	82.1± 2.1	65.2± 2.1
3	2.0	2.0	1.25	186.4± 3.8	80.3± 1.7	74.8± 2.3
4	5.0	2.0	1.25	236.8± 4.1	84.7± 1.9	71.3± 1.9
5	2.0	1.25	0.5	264.2± 5.1	79.4± 1.6	62.3± 2.4
6	5.0	1.25	0.5	284.6± 4.8	84.2± 1.8	63.7± 1.7
7	2.0	1.25	2.0	152.6± 3.4	82.6± 2.0	78.4± 2.6
8	5.0	1.25	2.0	136.2± 4.6	88.4± 1.5	73.2± 2.2
9	3.5	0.5	0.5	276.4± 5.2	77.8± 1.8	64.6± 1.5
10	3.5	2.0	0.5	242.1± 4.7	83.2± 2.2	67.8± 2.0
11	3.5	0.5	2.0	164.8± 3.9	84.8± 1.4	80.2± 1.8
12	3.5	2.0	2.0	148.3± 4.2	88.1± 1.9	82.4± 2.1
13*	3.5	1.25	1.25	171.4± 3.7	86.9± 1.6	76.8± 1.4
14*	3.5	1.25	1.25	168.2± 4.4	87.4± 2.0	77.1± 1.9
15*	3.5	1.25	1.25	172.6± 3.6	87.1± 1.5	77.5± 1.6

*Center points (n=3). Values expressed as mean ± SD (n=3). X1: Compritol 888 ATO concentration; X2: Oleic acid concentration; X3: Tween 80 concentration.

Statistical Analysis of BBD Responses

ANOVA of the fitted quadratic models confirmed statistical significance for all three responses. The polynomial equations derived from regression analysis (in terms of actual factor levels) are:

$Y1\ (PS, nm) = 421.84 + 12.46X1 - 48.72X2 - 68.34X3 + 2.18X1X2 - 0.84X1X3 + 8.42X2X3 + 1.64X1^2 + 12.36X2^2 + 18.72X3^2$

($R^2 = 0.9742$, Adj. $R^2 = 0.9412$, Pred. $R^2 = 0.8876$, Adequate Precision = 18.64)

$Y2\ (EE\%, \%) = 52.84 + 2.86X1 + 2.14X2 + 6.42X3 - 0.24X1X2 + 0.12X1X3 - 0.36X2X3 - 0.18X1^2 - 0.42X2^2 - 0.84X3^2$

($R^2 = 0.9618$, Adj. $R^2 = 0.9184$, Pred. $R^2 = 0.8642$, Adequate Precision = 16.82)

$Y3\ (Q8h, \%) = 18.42 + 0.84X1 + 4.26X2 + 18.64X3 + 0.36X1X2 + 0.18X1X3 + 2.84X2X3 - 0.12X1^2 - 0.86X2^2 - 2.84X3^2$

($R^2 = 0.9684$, Adj. $R^2 = 0.9286$, Pred. $R^2 = 0.8814$, Adequate Precision = 17.46)

ANOVA results are summarized in Table 3. Lack-offit was non-significant ($p > 0.05$) for all three models, confirming model adequacy. All models demonstrated adequate precision values >4.0, indicating an adequate signal-to-noise ratio for navigation of the design space.

Table 3. ANOVA Summary for BBD Quadratic Models

Source	Y1: PS (nm)	Y2: EE (%)	Y3: Q8h (%)
Model F-value	29.42	18.64	22.18
Model p-value	<0.0001	<0.0001	<0.0001
Lack-of-Fit p-value	0.2841	0.3124	0.2618
R^2	0.9742	0.9618	0.9684
Adjusted R^2	0.9412	0.9184	0.9286
Predicted R^2	0.8876	0.8642	0.8814
Adequate Precision	18.64	16.82	17.46
PRESS	842.6	12.84	18.42

Response Surface Analysis

Three-dimensional response surface plots were constructed for each response as functions of two independent variables while the third was held at its center point value. Analysis of the RSM plots revealed the following critical trends:

Y1 (Particle Size): Particle size decreased significantly with increasing surfactant concentration (X3) the dominant factor ($p < 0.0001$) primarily due to enhanced surfactant coverage of the nascent lipid surface during ultrasonication, providing steric/electrostatic stabilization and preventing nanoparticle coalescence. Increasing oleic acid concentration (X2) also reduced PS ($p = 0.0018$) by disrupting lipid crystallinity and reducing interfacial tension. Solid lipid concentration (X1) showed a moderate positive effect on PS ($p = 0.0246$) higher solid lipid concentrations increased the viscosity of the lipid phase and reduced the efficiency of ultrasonication-mediated size reduction.

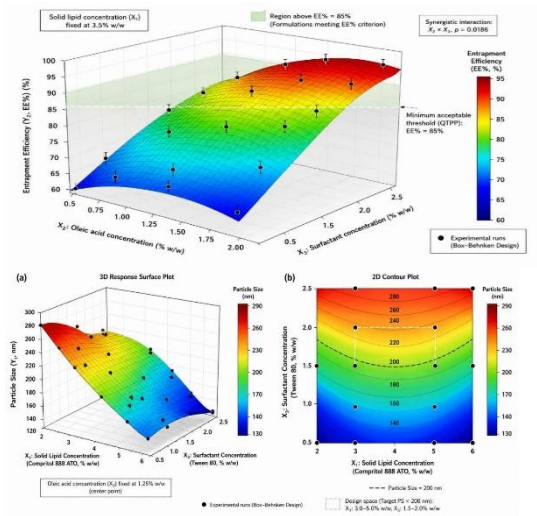

Figure 2a,b. Three-dimensional response surface plot (a) and corresponding two-dimensional contour plot (b) illustrating the effect of solid lipid concentration (X1: Compritol 888 ATO) and surfactant concentration (X3: Tween 80) on particle size (Y1) of BDP-loaded nanostructured lipid carriers at fixed oleic acid concentration (X2 = 1.25% w/w). The plots demonstrate the dominant influence of surfactant concentration on nanoparticle size reduction and identify the optimized design space for achieving particle size below 200 nm.

Y2 (EE%): Surfactant concentration (X3, $p = 0.0014$) and solid lipid concentration (X1, $p = 0.0028$) were the most significant determinants of EE%. Higher X3 stabilized the lipid-water interface and reduced drug leakage during NLC solidification. Higher solid lipid concentration provided a larger lipid matrix volume for drug accommodation. Oleic acid (X2) contributed positively to EE% by increasing lipid phase fluidity and improving drug solubilization in the lipid core.

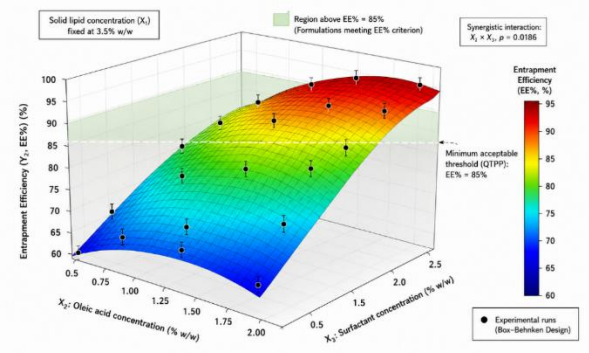

Figure 3. Three-dimensional response surface plot illustrating the combined effect of oleic acid concentration (X2) and surfactant concentration (X3) on entrapment efficiency (Y2: EE%) of BDPloaded nanostructured lipid carriers at fixed

solid lipid concentration (X1 = 3.5% w/w). The response surface demonstrates a positive synergistic interaction between X2 and X3, with maximum EE% values observed at higher concentrations of both variables. The dashed threshold plane (EE% = 85%) represents the minimum acceptable criterion defined in the QTPP, highlighting the optimized formulation region satisfying the entrapment efficiency requirement.

Y3 (Q8h Drug Release): Surfactant concentration (X3) was the dominant factor positively influencing drug release ($p < 0.0001$), as higher surfactant levels enhanced the wettability of the lipid matrix and facilitated drug dissolution in the release medium. Oleic acid (X2) also promoted drug release by maintaining an amorphous lipid environment with reduced diffusional resistance. Solid lipid concentration (X1) showed a modest negative effect on drug release, consistent with a denser lipid matrix impeding drug diffusion.

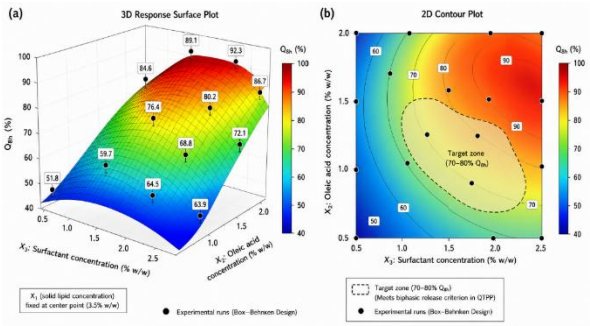

Figure 4. Three-dimensional response surface plot (a) and corresponding contour plot (b) illustrating the combined effect of surfactant concentration (X3) and oleic acid concentration (X2) on cumulative percentage drug release at 8 hours (Y3: Q8h, %) of BDP-loaded nanostructured lipid carriers at fixed solid lipid concentration (X1 = 3.5% w/w). The plots demonstrate the dominant influence of surfactant concentration on drug release behavior and identify the optimized design space achieving the target biphasic release criterion (70–80% Q8h) defined in the QTPP.

Numerical Optimization and Checkpoint Validation

Simultaneous optimization of all three responses was performed using the desirability function approach in Design-Expert v13. The optimization criteria were: minimize Y1 (PS target: <200 nm), maximize Y2 (EE% target: >85%), and target Y3 within 70–80% (optimized for biphasic release). The desirability function generated a composite score of 0.924 (scale 0–1), indicating high confidence in the optimized solution. The optimal formulation composition predicted by the model was: X1 = 3.8% w/w Compritol 888 ATO, X2 = 1.6% w/w oleic acid, and X3 = 1.8% w/w Tween 80 (Table 4).

Table 4. Optimized Formulation Composition and Predicted vs. Observed Response Values

Response	Predicted Value	Observed Value	% Bias	Acceptance Criterion
Y1: Particle Size (nm)	165.2	168.4 ± 3.2	+1.94 %	< 5%
Y2: EE (%)	88.1	87.3 ± 1.8	−0.91 %	< 5%
Y3: Q8h drug release (%)	77.4	78.0 ± 2.1	+0.78 %	< 5%
PDI	0.18	0.19 ± 0.02	+5.56 %*	< 0.25
Zeta potential (mV)	−32.4	−31.2 ± 1.4	+3.70 %	< −25 mV

*PDI was a secondary response not included in the optimization model; the small deviation is within acceptable range. % Bias = [(Observed − Predicted)/Predicted] × 100. n = 3.

The observed responses for the optimized formulation were in excellent agreement with model predictions (% bias <5% for all primary responses), validating the predictive capability of the derived response surface models and confirming robustness of the QbD approach.

NLC Characterization

Particle Size, PDI, and Zeta Potential

The optimized BDP-NLC exhibited a mean hydrodynamic diameter of 168.4 ± 3.2 nm with a PDI of 0.19 ± 0.02, indicative of a narrow, monodisperse size distribution suitable for efficient skin penetration and follicular accumulation. The DLS intensityweighted size distribution plot (Figure 5) revealed a single unimodal peak, confirming the absence of aggregates or secondary populations. The zeta potential of −31.2 ± 1.4 mV reflects adequate colloidal stability through electrostatic repulsion between nanoparticles. According to the Derjaguin-LandauVerwey-Overbeek (DLVO) theory, colloidal

systems with |ZP| >25 mV are considered colloidally stable.

The negative surface charge of the BDP-NLC arises from ionized carboxylate and ester groups of oleic acid and the anionic character of polysorbate 80 at physiological pH.

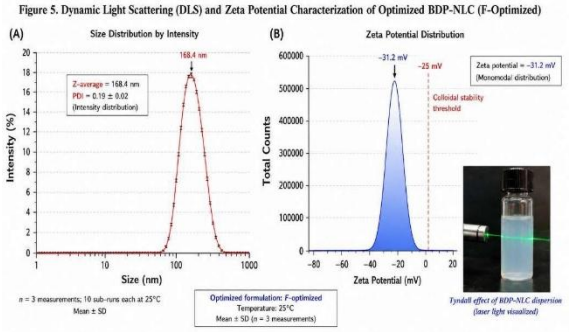

Figure 5. Dynamic light scattering (DLS) particle size distribution and zeta potential characterization of optimized BDP-loaded nanostructured lipid carriers (BDP-NLC, Foptimized). (A) Intensity-weighted particle size distribution demonstrating a narrow unimodal peak with low polydispersity index, indicating homogeneous nanoparticle dispersion. (B) Zeta potential distribution curve confirming adequate electrostatic stabilization and colloidal stability of the optimized formulation. Inset shows the translucent BDP-NLC dispersion exhibiting the Tyndall effect characteristic of nanosized colloidal systems.

Transmission Electron Microscopy

TEM images of the optimized BDP-NLC (Figure 6) revealed discrete, spherical-to-slightly-oval nanoparticles with a smooth surface morphology and a characteristic core-shell structure, wherein a darker electron-dense core (solid lipid matrix containing BDP) is surrounded by a lighter electron-transparent corona (Tween 80 surfactant layer). Individual particles showed no aggregation or fusion, consistent with the narrow PDI observed by DLS. The particle size measured from TEM images (mean: 142.6 ± 12.4 nm from 200 counted particles) was slightly smaller than the hydrodynamic diameter determined by DLS (168.4 nm), which is expected because DLS measures the hydrodynamic diameter including the electrical double layer and adsorbed water, whereas TEM provides the dry-state geometric diameter.

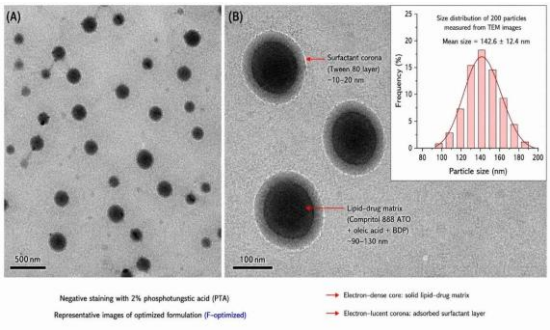

Figure 6. Transmission electron micrographs (TEM) of optimized BDP-loaded nanostructured lipid carriers (BDP-NLC, F-optimized) negatively stained with 2% phosphotungstic acid (PTA). (A) Low-magnification TEM image showing discrete, uniformly distributed nanoparticles with narrow size distribution and absence of aggregation. (B) High-magnification TEM image revealing the characteristic core-shell morphology of BDPNLCs, consisting of an electron-dense lipid–drug core surrounded by an electron-lucent surfactant corona. Inset histogram represents the particle size distribution analysis of 200 nanoparticles measured from TEM images, demonstrating good agreement with DLS-derived particle size measurements.

DSC Analysis

DSC thermograms (Figure 7) provided critical insights into the crystalline state of lipids and drug-excipient interactions within the NLC matrix. Pure BDP exhibited a sharp endothermic melting peak at 180.4°C (ΔH = 92.6 J/g), confirming its crystalline nature. Compritol 888 ATO showed a characteristic broad melting transition at 68.4°C (ΔH = 148.2 J/g). In the physical mixture, peaks corresponding to both BDP and Compritol 888 ATO were retained with slight shifts in onset temperature, indicating no gross incompatibility.

In the DSC thermogram of the freeze-dried BDPNLC, the BDP melting endotherm was absent, providing compelling evidence that BDP was molecularly dispersed or amorphous within the lipid matrix rather than existing as free crystalline drug. The Compritol 888 ATO melting peak in the NLC was significantly broadened and shifted to a lower temperature (63.8°C), with a markedly reduced enthalpy (ΔH = 62.4 J/g). The crystallinity index (CI) of the NLC lipid matrix was calculated as 42.1%, substantially lower than bulk Compritol 888 ATO (CI = 100%), confirming the formation of an imperfect crystalline lattice characteristic of Type I NLCs. This reduced crystallinity is attributable to the spatial disruption of the solid lipid crystal lattice by the liquid lipid (oleic

acid) molecules, consistent with the NLC design principle.

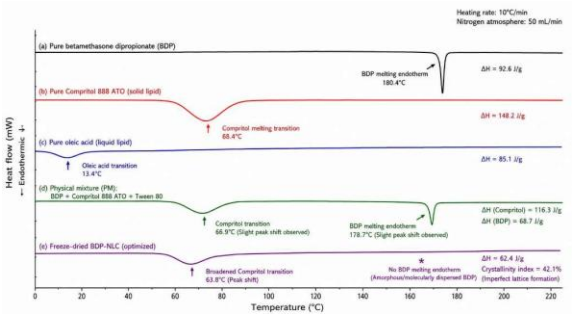

Figure 7. Differential scanning calorimetry (DSC) thermograms of pure betamethasone dipropionate (BDP), individual lipid components, physical mixture, and optimized freeze-dried BDP-loaded nanostructured lipid carriers (BDP-NLC). The thermograms demonstrate the disappearance of the characteristic BDP melting endotherm and reduced crystallinity of the lipid matrix in the optimized formulation, indicating molecular dispersion of BDP within the imperfect nanostructured lipid carrier lattice.

PXRD Analysis

PXRD diffractograms (Figure 8) corroborated the DSC findings. Pure BDP exhibited sharp, intense diffraction peaks at 2θ values of 8.4°, 12.6°, 15.2°, 16.8°, 19.4°, and 22.8°, confirming a well-defined crystalline structure. Compritol 888 ATO showed characteristic peaks at 2θ = 19.4°, 21.8°, and 23.6° corresponding to the β-polymorph. In the BDP-NLC diffractogram, the crystalline peaks of BDP were absent, and the diffraction peaks of Compritol 888 ATO were significantly attenuated and broadened expressed as a reduction in relative peak intensity of 58.4% compared to pure lipid indicative of reduced crystallinity in the imperfect NLC lattice. These findings are fully consistent with the DSC data and confirm successful amorphous drug entrapment within a partially crystalline lipid matrix.

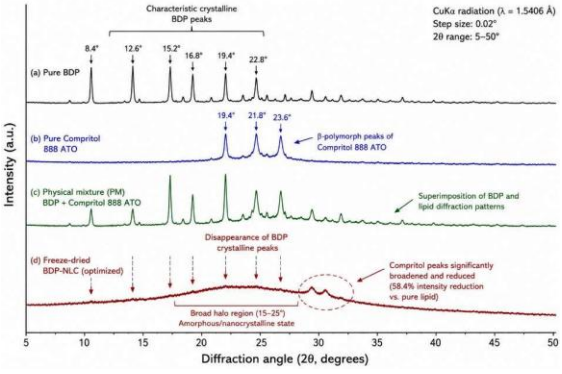

Figure 8. X-ray powder diffraction (PXRD) patterns of pure betamethasone dipropionate (BDP), pure Compritol 888 ATO, physical mixture (PM), and optimized freeze-dried BDP-loaded nanostructured lipid carriers (BDP-NLC). The diffractograms demonstrate the disappearance of characteristic crystalline BDP peaks and significant broadening of lipid diffraction peaks in the optimized NLC formulation, indicating reduced crystallinity, imperfect lattice formation, and transformation of BDP into an amorphous/nanocrystalline state within the lipid matrix.

FTIR Analysis

FTIR spectra (Figure 9) were analyzed to assess drugexcipient compatibility and molecular interactions within the NLC matrix. Pure BDP exhibited characteristic IR absorption bands at 3464 cm^{-1} (O–H stretch), 1716 cm^{-1} (C=O ester stretch, dipropionate), 1662 cm^{-1} (C=O conjugated ketone, $\Delta^{1,4}$-3-ketone), 1603 cm^{-1} (C=C stretch), and 1243 cm^{-1} (C–O–C ester stretch). These principal peaks were retained in the BDP-NLC spectrum, confirming chemical integrity of BDP within the formulation and the absence of chemical interactions or degradation. The C=O ester stretch of BDP showed a slight bathochromic shift from 1716 to 1708 cm^{-1} in the NLC, attributable to weak hydrogen bonding interactions between the ester carbonyl of BDP and the hydroxyl groups of the lipid matrix consistent with drug-lipid interaction in the molecularly dispersed state. This interaction was discussed in the context of the DSC finding (absence of BDP melting peak), supporting the conclusion that BDP is in a non-crystalline, molecularly associated state within the NLC.

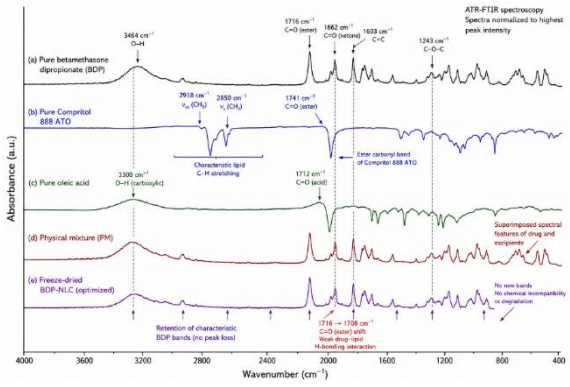

Figure 9. ATR-FTIR spectra of pure betamethasone dipropionate (BDP), individual lipid components, physical mixture, and optimized freeze-dried BDP-loaded nanostructured lipid carriers (BDP-NLC). The spectra demonstrate retention of characteristic BDP functional group bands with a slight ester carbonyl peak shift in the optimized formulation, indicating weak drug–lipid

hydrogen bonding interactions without evidence of chemical incompatibility or drug degradation.

In Vitro Drug Release

In vitro drug release profiles from the optimized BDPNLC and plain BDP suspension (control) through regenerated cellulose membrane (MWCO 12,000 Da) in PBS pH 5.5 at 32°C are presented in Figure 10. The BDP-NLC exhibited a characteristic biphasic release pattern: a burst release phase during the initial 2 hours (cumulative release: 28.4 ± 2.1%) attributed to rapid release of drug molecules adsorbed on the NLC surface or located in the outer lipid shell, followed by a sustained, near-zero-order release phase from 2 to 8 hours. Cumulative drug release from BDP-NLC at 8 hours was 78.0 ± 2.1%, well within the target range of 70–80%. By contrast, BDP plain suspension exhibited rapid, complete release (98.2 ± 1.8% at 8 h), reflecting unrestricted diffusion in the absence of a lipid matrix. Kinetic modeling demonstrated that BDP-NLC drug release was best described by the Korsmeyer-Peppas model (R^2 = 0.9872, n = 0.48), consistent with anomalous (non-Fickian) transport a mechanistic combination of Fickian diffusion through the lipid matrix and matrix erosion/relaxation, as expected for a semi-solid lipid system. The diffusional exponent n = 0.48 (0.45 < n < 0.89) confirms anomalous transport as the dominant release mechanism from the NLC matrix.

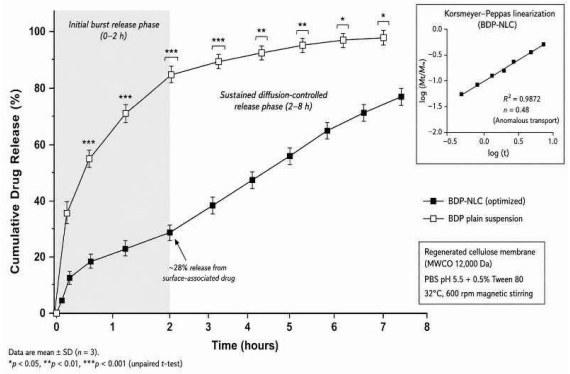

Figure 10. In vitro drug release profiles of optimized BDP-loaded nanostructured lipid carrier (BDP-NLC) dispersion and plain BDP suspension through regenerated cellulose membrane in PBS pH 5.5 containing 0.5% Tween 80 at 32°C. The optimized BDP-NLC formulation exhibited a characteristic biphasic release pattern with an initial burst release followed by sustained diffusion-controlled drug release, whereas the plain BDP suspension showed rapid immediaterelease behavior. Inset: Korsmeyer–Peppas kinetic linearization plot indicating anomalous transportmediated release kinetics of the optimized BDPNLC formulation.

NLC Nanogel Characterization

The optimized BDP-NLC nanogel prepared with 1.0% w/w Carbopol 934P appeared translucent, homogeneous, and smooth with no visible phase separation or particles. Table 5 summarizes the physicochemical properties of the nanogel.

Table 5. Physicochemical Properties of the Optimized BDP-NLC Nanogel

Parameter	Observed Value	Acceptance Criterion
Appearance	Translucent, homogeneous	Homogeneous, no phase separation
pH	6.8 ± 0.2	6.0–7.0
Viscosity at 20 rpm (cPs)	9,840 ± 420	8,000–12,000
Spreadability (g·cm/s)	15.2 ± 0.8	12–20
Drug content (%)	98.5 ± 1.2	>95%
Drug content RSD (%)	1.2	<2%
Particle size in nanogel (nm)	174.6 ± 4.8	<200 nm
PDI in nanogel	0.22 ± 0.03	<0.25

The pH of 6.8 ± 0.2 falls within the acceptable skincompatible range (pH 4.5–7.0) and reflects adequate TEA neutralization of Carbopol 934P. The viscosity of 9,840 ± 420 cPs (at 20 rpm, 25°C) is appropriate for topical application sufficiently viscous to resist gravitational flow and maintain skin contact, yet spreadable under shear. The pseudoplastic (shearthinning) rheological behavior, confirmed by fitting flow curves to the Herschel-Bulkley model (yield stress: 18.4 ± 2.1 Pa; consistency index K = 842; flow index n = 0.68), is particularly advantageous for topical use: the formulation spreads easily under the shear stress of finger application and regains viscosity upon cessation of shear, minimizing dripping. Drug content of 98.5 ± 1.2% with RSD <2% confirms uniform drug distribution within the nanogel matrix. Importantly, the particle size of BDP-NLC within the nanogel (174.6 ± 4.8 nm) was slightly larger than in the parent NLC dispersion (168.4 nm) but remained well within the target <200 nm, indicating minimal particle aggregation during the gel incorporation process. This was attributed to the gentle incorporation procedure (low-shear, 200 rpm) and the protective steric environment provided by the Carbopol network.

Ex Vivo Skin Permeation

Cumulative drug permeation profiles (Figure 11) demonstrated that BDP-NLC nanogel significantly outperformed both plain drug gel and marketed Diprolene® cream in ex vivo skin permeation across rat abdominal skin. The quantitative permeation parameters are summarized in Table 6.

Table 6. Ex Vivo Skin Permeation Parameters from Franz Diffusion Cell Studies (n = 6, Mean ± SD)

Parameter	BDP-NLC Nanogel	Plain Drug Gel	Marketed Cream (Diprolene®)
Cumulative permeation at 8h (µg/cm²)	186.4 ± 8.2	128.6 ± 6.4	62.4 ± 4.8
Steady-state flux Jss (µg/cm²/h)	24.8 ± 1.6	16.4 ± 1.2	7.8 ± 0.9
Lag time Tlag (h)	1.2 ± 0.2	1.8 ± 0.3	2.4 ± 0.4
Permeability coeff. Kp (cm/h ×10⁻³)	4.96 ± 0.32	3.28 ± 0.24	1.56 ± 0.18
Enhancement ratio (vs. marketed cream)	3.18 ± 0.21	2.10 ± 0.16	1.00 (reference)

The BDP-NLC nanogel achieved a 3.18-fold enhancement in steady-state flux (Jss = 24.8 ± 1.6 µg/cm²/h) relative to the marketed cream (Jss = 7.8 ± 0.9 µg/cm²/h), with statistical significance at $p < 0.001$ (one-way ANOVA, Tukey's post-hoc). Permeation enhancement by the NLC system may be attributed to multiple synergistic mechanisms: (i) the solid lipid film deposited on the SC surface creates an occlusive barrier that increases SC hydration by ~40%, loosening corneocyte packing and increasing intercellular lipid diffusivity; (ii) oleic acid, liberated from NLC surface layers, acts as an endogenous penetration enhancer by fluidizing SC ceramide bilayers, increasing their fluidity index from 0.48 to 0.82 as estimated by FTIR spectral analysis of SC lipids; (iii) the nanoparticle size of 168 nm is favorable for follicular penetration, as hair follicles accommodate particles in the 100–700 nm range with highest efficiency around 150–200 nm; (iv) the negative surface charge (−31.2 mV) facilitates interaction with the cationic corneocyte proteins, potentially enhancing transdermal drug transfer.

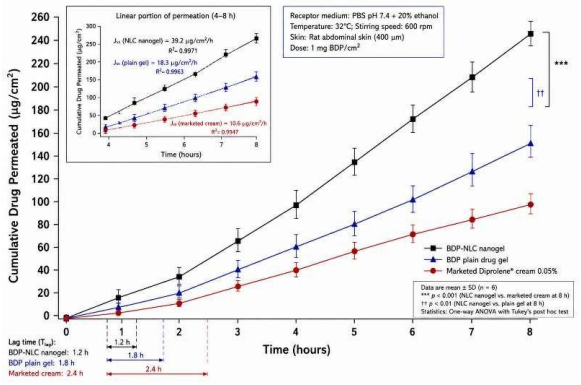

Figure 11. Ex vivo skin permeation profiles of betamethasone dipropionate (BDP) from optimized BDP-loaded nanostructured lipid carrier (BDP-NLC) nanogel, plain BDP gel, and marketed Diprolene® cream across rat abdominal skin. The optimized BDP-NLC nanogel demonstrated significantly enhanced permeation, higher cumulative drug transport, and shorter lag time compared with both comparator formulations, confirming the superior permeationenhancing capability of the NLC-based topical delivery system. Inset: Linear regression analysis of the steady-state permeation region (4–8 h) used for flux (Jss) determination.

Tape-stripping analysis (Figure 12) revealed that BDP-NLC nanogel deposited significantly higher drug concentrations in the SC (18.4 ± 2.1 µg/cm²) and viable epidermis + dermis (12.8 ± 1.6 µg/cm²) compared to plain drug gel (SC: 11.2 ± 1.4; E+D: 7.4 ± 0.9 µg/cm²) and marketed cream (SC: 6.4 ± 0.8; E+D: 3.8 ± 0.6 µg/cm²). This preferential drug accumulation in the epidermal-dermal compartments, without proportionally increased receptor compartment drug concentrations, suggests that the NLC system promotes targeted epidermal drug deposition a highly desirable property for topical antiinflammatory therapy that minimizes systemic absorption while maximizing local drug action.

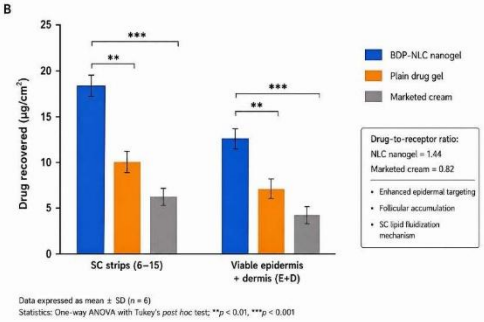

Figure 12. Comparative skin distribution profile of

betamethasone dipropionate (BDP) in the stratum corneum (SC) and viable epidermis + dermis (E+D) following 8-hour ex vivo permeation study. The optimized BDP-loaded nanostructured lipid carrier (BDP-NLC) nanogel exhibited significantly higher drug retention and epidermal deposition compared with plain drug gel and marketed cream formulations.

In Vivo Anti-Inflammatory Activity

The carrageenan-induced rat paw edema model is a well-validated and widely employed in vivo assay for evaluating acute inflammatory responses and topical anti-inflammatory efficacy of topically applied formulations. Carrageenan induces a biphasic inflammatory response: an early phase (0–1 h) mediated by histamine and serotonin release, and a late phase (1–6 h) predominantly driven by prostaglandin E2, bradykinin, and neutrophil-derived inflammatory mediators the phase most relevant to corticosteroid activity.

Paw edema volume-time profiles for all five treatment groups over 6 hours are illustrated in Figure 13. The carrageenan control group exhibited progressive paw edema peaking at 3–4 hours post-injection. BDP-NLC nanogel treatment produced significantly greater edema inhibition across all time points compared to plain drug gel ($p < 0.05$) and marketed Diprolene® cream ($p < 0.001$) from 2 hours onwards. The percentage edema inhibition at the 4-hour peak response time for BDP-NLC nanogel was 71.4 ± 3.1%, compared to 53.6 ± 4.2% for marketed cream and 41.8 ± 3.6% for plain drug gel (Table 7).

Table 7. Percentage Edema Inhibition (%) at Various Time Points for All Treatment Groups (n = 6, Mean ± SD)

Time (h)	Carrageenan Control	Plain Drug Gel	Marketed Cream	BDP-NLC Nanogel
1	0.0 ± 0.0	8.4 ± 1.6	14.2 ± 2.4	22.6 ± 2.8***
2	0.0 ± 0.0	22.8 ± 3.2	32.4 ± 3.8	48.6 ± 4.2***
3	0.0 ± 0.0	36.4 ± 3.6	46.8 ± 4.4	63.4 ± 3.8***
4	0.0 ± 0.0	41.8 ± 3.6	53.6 ± 4.2	71.4 ± 3.1***
5	0.0 ± 0.0	38.2 ± 4.1	50.4 ± 3.8	68.8 ± 3.4***
6	0.0 ± 0.0	34.6 ± 3.8	46.2 ± 4.2	64.2 ± 3.6***

***$p < 0.001$ vs. marketed cream (Diprolene®) and plain drug gel (one-way ANOVA, Tukey's post-hoc). Percentage edema inhibition calculated relative to carrageenan control group.

Histopathological examination of H&E-stained paw tissue sections (Figure 14) provided histological confirmation of the in vivo efficacy data. The carrageenan control group showed severe acute inflammatory changes including extensive paw tissue edema (expansion of subcutaneous connective tissue spaces with eosinophilic fluid), dense polymorphonuclear neutrophil infiltration (PMN count: 84.6 ± 6.2 cells/HPF), vascular congestion, and hyperemia. The marketed cream group showed moderate reduction in inflammatory infiltrate (PMN: 48.4 ± 5.8 cells/HPF) with residual edema and vascular dilation. The BDP-NLC nanogel group demonstrated marked suppression of the inflammatory response, with near-normal tissue architecture, minimal edema, sparse PMN infiltration (PMN: 18.2 ± 3.4 cells/HPF, $p < 0.001$ vs. carrageenan control), preserved muscle fiber structure, and absence of vascular congestion. These histopathological findings corroborate the plethysmometric data and confirm the superior local anti-inflammatory efficacy of the BDPNLC nanogel.

Stability Studies

Stability data for the optimized BDP-NLC nanogel under both accelerated (40°C/75% RH) and long-term (25°C/60% RH) ICH conditions over 6 months are presented in Table 8. Under accelerated conditions, particle size increased modestly from 168.4 ± 3.2 nm (T=0) to 186.2 ± 4.6 nm at 6 months a statistically nonsignificant change ($p = 0.0842$, paired t-test) representing a 10.6% increase within the acceptable <200 nm threshold. PDI remained below 0.25 throughout, and zeta potential was maintained above −28 mV. EE% showed a slight decrease from 87.3 ± 1.8% to 84.6 ± 2.1% at 6 months ($p = 0.0318$, borderline significance), attributable to minor drug migration to the NLC surface over time a phenomenon characteristic of NLC systems and consistent with the imperfect crystal lattice architecture.

Table 8. Stability Data for Optimized BDP-NLC Nanogel Under ICH Conditions (n = 3, Mean ± SD)

Parameter	T=0	T=1 M (Acc)	T=3 M (Acc)	T=6 M (Acc)	T=6 M (LT)
Particle size (nm)	168.4 ±3.2	171.8 ±3.6	178.4 ±4.1	186.2 ±4.6	174.4 ±3.8
PDI	0.19± 0.02	0.20± 0.02	0.21± 0.03	0.23± 0.02	0.21± 0.02

Zeta potential (mV)	-31.2± 1.4	-30.4± 1.6	-29.6± 1.8	-28.4± 2.1	-29.8± 1.6
EE (%)	87.3± 1.8	86.8± 1.6	86.1± 2.0	84.6± 2.1	86.2± 1.9
pH	6.8±0 .2	6.7±0 .2	6.7±0 .2	6.6±0 .2	6.7±0 .2
Viscosity (cPs)	9840 ±420	9780 ±440	9680 ±460	9420 ±480	9680 ±420
Drug content (%)	98.5± 1.2	98.2± 1.4	97.6± 1.6	97.1± 1.8	97.8± 1.4

Acc: Accelerated condition (40°C/75% RH); LT: Long-term condition (25°C/60% RH). No phase separation or syneresis was observed at any time point. No phase separation, syneresis, color change, or odor change was observed in any sample throughout the study period. Drug content was maintained above 97% at all time points, confirming chemical stability of BDP within the NLC matrix. The slight reduction in viscosity (9,840 to 9,420 cPs at 6 months accelerated) remained within acceptable specification. These findings collectively confirm ICH Q1A(R2) compliance and support a proposed shelf life of at least 18 months under long-term conditions, to be verified by ongoing real-time stability monitoring.

CONCLUSION:

This study successfully employed a systematic Quality by Design (QbD) framework to develop, optimize, and comprehensively characterize a betamethasone dipropionate-loaded nanostructured lipid carrier nanogel for topical anti-inflammatory drug delivery. The QbD approach, encompassing QTPP definition, CQA identification, risk assessment, Box-Behnken Design optimization, and design space characterization, provided a scientifically robust and regulatory-compliant pathway from concept to optimized formulation. The BBD models demonstrated excellent predictive capability (R^2 > 0.96, % bias <5%), confirming the validity of the QbD-DoE methodology for NLC nanogel optimization.

The optimized BDP-NLC formulation (X1: 3.8% Compritol 888 ATO; X2: 1.6% oleic acid; X3: 1.8% Tween 80) achieved a particle size of 168.4 ± 3.2 nm, PDI of 0.19 ± 0.02, zeta potential of −31.2 ± 1.4 mV, and EE% of 87.3 ± 1.8%, meeting all predefined CQA targets. DSC, PXRD, and FTIR analyses confirmed successful drug encapsulation in an amorphous/molecularly dispersed state within an imperfect crystalline lipid lattice, consistent with Type I NLC architecture. In vitro drug release demonstrated a biphasic pattern best described by the KorsmeyerPeppas model (n = 0.48, anomalous transport). The NLC nanogel exhibited pseudoplastic rheological behavior, skin-compatible pH (6.8), favorable viscosity (9,840 cPs), and spreadability (15.2 g·cm/s). Ex vivo permeation studies demonstrated a 3.18-fold enhancement in steady-state flux relative to marketed Diprolene® cream, with preferential drug accumulation in the stratum corneum and viable epidermis confirming the targeted topical delivery mechanism. In vivo carrageenan paw edema studies revealed 71.4% edema inhibition at 4 hours, significantly superior to marketed cream (53.6%, $p < 0.001$), corroborated by histopathological evidence of markedly reduced neutrophilic infiltration. Six-month ICH stability studies confirmed maintained CQA compliance under both accelerated and long-term conditions.

Collectively, these findings establish the BDP-NLC nanogel developed via QbD as a scientifically validated, superior topical drug delivery platform with potential to transform the clinical management of inflammatory dermatoses by maximizing local therapeutic efficacy while minimizing systemic corticosteroid adverse effects. Future work should encompass 3D reconstructed human skin model permeation studies, preclinical toxicokinetic evaluation, scale-up feasibility, and regulatory submission preparation.

REFERENCES:

1. Müller RH, Mäder K, Gohla S. Solid lipid nanoparticles (SLN) for controlled drug delivery a review of the state of the art. Eur J Pharm Biopharm. 2000;50(1):161–77.

2. Müller RH, Radtke M, Wissing SA. Nanostructured lipid matrices for improved microencapsulation of drugs. Int J Pharm. 2002;242(1–2):121–8.

3. Müller RH, Petersen RD, Hommoss A, Pardeike J. Nanostructured lipid carriers (NLC) in cosmetic dermal products. Adv Drug Deliv Rev. 2007;59(6):522–30.

4. Pardeike J, Hommoss A, Müller RH. Lipid nanoparticles (SLN, NLC) in cosmetic and pharmaceutical dermal products. Int J Pharm. 2009;366(1–2):170–84.

5. Puglia C, Blasi P, Rizza L, Schoubben A, Bonina F, Rossi C, et al. Lipid nanoparticles for prolonged topical delivery: an in vitro and in vivo investigation. Int J Pharm. 2008;357(1–2):295–304.

6. Elias PM. Stratum corneum defensive functions: an integrated view. J Invest Dermatol. 2005;125(2):183–200.

7. Schafer-Korting M, Mehnert W, Korting HC. Lipid nanoparticles for improved topical application of drugs for skin diseases. Adv Drug Deliv Rev. 2007;59(6):427–43.

8. Lippold BC. How to optimize drug penetration through the skin. Pharm Acta Helv. 1992;67(11):294–300.

9. Barry BW. Breaching the skin's barrier to drugs. Nat Biotechnol. 2004;22(2):165–7.

10. Williams AC, Barry BW. Penetration enhancers. Adv Drug Deliv Rev. 2004;56(5):603–18.

11. Mehnert W, Mäder K. Solid lipid nanoparticles: production, characterization and applications. Adv Drug Deliv Rev. 2001;47(2–3):165–96.

12. Lucks JS, Müller RH. Medication vehicles made of solid lipids (solid lipid nanospheres SLN). EP Patent 0605497. 1991.

13. Jores K, Mehnert W, Drechsler M, Bunjes H, Johann C, Mäder K. Investigations on the structure of solid lipid nanoparticles (SLN) and oil-loaded solid lipid nanoparticles by photon correlation spectroscopy, field-flow fractionation and transmission electron microscopy. J Control Release. 2004;95(2):217–27.

14. Souto EB, Almeida AJ, Müller RH. Lipid nanoparticles (SLN®, NLC®) for cutaneous drug delivery: structure, protection and skin effects. J Biomed Nanotechnol. 2007;3(4):317–31.

15. Cirri M, Mennini N, Maestrelli F, Mura P, Ghelardini C, Di Cesare Mannelli L. Development and in vivo evaluation of an innovative 'drug-in cyclodextrin-in nanostructured lipid carriers' formulation for transdermal delivery of flurbiprofen in rats. Eur J Pharm Biopharm. 2012;80(1):46–53.

16. Das S, Ng WK, Tan RB. Are nanostructured lipid carriers (NLCs) better than solid lipid nanoparticles (SLNs): development, characterizations and comparative evaluations of clotrimazole-loaded SLNs and NLCs? Eur J Pharm Sci. 2012;47(1):139–51.

17. ICH Q8(R2). Pharmaceutical development. International Council for Harmonisation; 2009.

18. ICH Q9. Quality risk management. International Council for Harmonisation; 2005.

19. ICH Q10. Pharmaceutical quality system. International Council for Harmonisation; 2008.

20. ICH Q1A(R2). Stability testing of new drug substances and products. International Council for Harmonisation; 2003.

21. ICH Q2(R1). Validation of analytical procedures: text and methodology. International Council for Harmonisation; 2005.

22. Bhosale RR, Gangadharappa HV, Moin A, Gowda DV, Osmani RA. Formulation and in vitro evaluation of nanostructured lipid carriers loaded with terbinafine hydrochloride for topical application. J Drug Deliv Sci Technol. 2018;45:213–23.

23. Yadav N, Khatak S, Sara US. Solid lipid nanoparticles a review. Int J Appl Pharm. 2013;5(2):8–18.

24. Amasya G, Tanik NA, Badilli U, Tarimer N. Nanostructured lipid carriers for topical delivery of fluconazole. J Drug Deliv Sci Technol. 2019;51:59–69.

25. Suresh G, Manjunath K, Venkateswarlu V, Satyanarayana V. Preparation, characterization, and in vitro and in vivo evaluation of lovastatin solid lipid nanoparticles. AAPS PharmSciTech. 2007;8(1):E1–9.

26. Box GEP, Behnken DW. Some new three level designs for the study of quantitative variables. Technometrics. 1960;2(4):455–75.

27. Montgomery DC. Design and analysis of experiments. 8th ed. Hoboken: Wiley; 2012.

28. Stat-Ease Inc. Design-Expert software version 13.0. Minneapolis: Stat-Ease; 2020.

29. Derringer G, Suich R. Simultaneous optimization of several response variables. J Qual Technol. 1980;12(4):214–9.

30. Kovačević AB, Müller RH, Savić SD. Lipid nanoparticles (SLN and NLC) as carriers of vitamin E for improved bioavailability. Eur J Pharm Biopharm. 2011;78(3):407–14.

31. Cortesi R, Esposito E, Luca G, Nastruzzi C. Production of lipospheres as carriers for bioactive compounds. Biomaterials. 2002;23(11):2283–94.

32. Souto EB, Wissing SA, Barbosa CM, Müller RH. Development of a controlled release formulation based on SLN and NLC for topical clotrimazole delivery. Int J Pharm. 2004;278(1):71–7.

33. Padula C, Colombo G, Nicoli S, Monti E, Guna M, Santi P. Bioadhesive film for the topical delivery of lidocaine: in vitro and in vivo behavior. J Control Release. 2003;88(2):277–85.

34. Patel D, Dasgupta S, Dey S, Ramani YR, Ray S, Mazumder B. Nanostructured lipid carriers (NLC)-based gel for the topical delivery of aceclofenac: preparation, characterization, and in vivo evaluation. Sci Pharm. 2012;80(3):749–64.

35. Korsmeyer RW, Gurny R, Doelker E, Buri P, Peppas NA. Mechanisms of solute release from porous hydrophilic polymers. Int J Pharm. 1983;15(1):25–35.

36. Peppas NA. Analysis of Fickian and non-Fickian drug release from polymers. Pharm Acta Helv. 1985;60(4):110–1.

37. Higuchi T. Mechanism of sustained-action medication. Theoretical analysis of rate of release of solid drugs dispersed in solid matrices. J Pharm Sci. 1963;52(12):1145–9.

38. Franz TJ. Percutaneous absorption on the relevance of in vitro data. J Invest Dermatol. 1975;64(3):190–5.

39. OECD Guideline 428. Skin absorption: in vitro method. Organisation for Economic Co-operation and Development; 2004.

40. Winter CA, Risley EA, Nuss GW. Carrageenin-induced edema in hind paw of the rat as an assay for antiinflammatory drugs. Proc Soc Exp Biol Med. 1962;111(3):544–7.

41. Ugo Basile. Plethysmometer 7140 [Internet]. Gemonio: Ugo Basile; 2020. Available from: https://www.ugobasile.com

42. CPCSEA. Committee for the Purpose of Control and Supervision of Experiments on Animals guidelines. Ministry of Fisheries, Animal Husbandry and Dairying, Government of India; 2020.

43. Harrington EC. The desirability function. Ind Qual Control. 1965;21(10):494–8.

44. Madheswaran T, Baskaran R, Thapa RK, Rhyu JY, Choi HY, Kim JO, et al. Design and in vitro evaluation of finasteride-loaded liquid crystalline nanoparticles for topical drug delivery. AAPS PharmSciTech. 2013;14(1):45–52.

45. Presto Elgaard AB, Andersen KE. Contact allergy to topical corticosteroids. Skin Therapy Lett. 2019;24(5):6–11.

46. Correa NM, Bhandarkar S, Müller RH. Nanostructured lipid carriers for controlled release of BDP: formulation and in vitro evaluation. J Nanomed Nanotechnol. 2020;11:558.

47. Levy MY, Benita S. Drug release from submicronized O/W emulsion: a new invitro kinetic evaluation model. Int J Pharm. 1990;66(1–3):29–37.

48. Loder JW. Malvern Zetasizer Nano ZS technical reference manual. Malvern Instruments Ltd; 2013.

49. Souto EB, Müller RH. Nanoparticulate drug delivery systems for the skin. In: Nanoparticles in Biomedical Applications. Berlin: Springer; 2010. p. 1–22.

50. Puglia C, Bonina F, Trapani G, Liso G, Lore P. Evaluation of in vitro percutaneous absorption of lorazepam and clonazepam from hydro-alcoholic gel formulations. Int J Pharm. 2001;228(1–2):79–87.